The Astrophysical Journal, 750:86 (7pp), 2012 May 1 doi:10.1088/0004-637X/750/1/86

A *SPITZER SPACE TELESCOPE* STUDY OF THE DEBRIS DISKS AROUND FOUR SDSS WHITE DWARFS

C. S. Brinkworth[1,2], B. T. Gänsicke[3], J. M. Girven[1,3], D. W. Hoard[1], T. R. Marsh[3], S. G. Parsons[3], and D. Koester[4]
[1] Spitzer Science Center, California Institute of Technology, Pasadena, CA 91125, USA
[2] NASA Exoplanet Science Institute, California Institute of Technology, Pasadena, CA 91125, USA
[3] Department of Physics and Astronomy, University of Warwick, Warwick CV4 7AL, UK
[4] Institut für Theoretische Physik und Astrophysik, University of Kiel, 24098 Kiel, Germany
Received 2011 May 13; accepted 2012 February 28; published 2012 April 17

ABSTRACT

We present *Spitzer Space Telescope* data of four isolated white dwarfs that were previously known to harbor circumstellar gaseous disks. Infrared Array Camera photometry shows a significant infrared excess in all of the systems, SDSS0738+1835, SDSS0845+2257, SDSS1043+0855, and SDSS1617+1620, indicative of a dusty extension to those disks. The 4.5 μm excesses seen in SDSS0738, SDSS0845, and SDSS1617 are 7.5, 5.7, and 4.5 times the white dwarf contribution, respectively. In contrast, in SDSS1043, the measured flux density at 4.5 μm is only 1.7 times the white dwarf contribution. We compare the measured IR excesses in the systems to models of geometrically thin, optically thick disks, and find that we are able to match the measured spectral energy distributions to within 3σ of the uncertainties, although disks with unfeasibly hot inner dust temperatures generally provide a better fit than those below the dust sublimation temperature. Possible explanations for the dearth of dust around SDSS1043+0855 are briefly discussed. Including our previous study of SDSS1228+1040, all five white dwarfs with gaseous debris disks have significant amounts of dust around them. It is evident that gas and dust can coexist around these relatively warm, relatively young white dwarfs.

Key words: circumstellar matter – infrared: stars – stars: individual (SDSS J104341.53+085558.2, SDSS J084539.17+225728.0, SDSS J161717.04+162022.4, SDSS J073842.57+183509.6) – white dwarfs

1. INTRODUCTION

Since the discovery of the first dusty disk around the white dwarf G29-39 (Zuckerman & Becklin 1987; Graham et al. 1990; Telesco et al. 1990; Tokunaga et al. 1990; Reach et al. 2005; von Hippel et al. 2007), dust disks have been detected around at least 26 isolated white dwarfs (Jura 2003, 2008; Kilic et al. 2005, 2006, 2011; Becklin et al. 2005; Jura et al. 2007; von Hippel et al. 2007; Kilic & Redfield 2007; Farihi et al. 2008, 2009, 2010, 2012; Brinkworth et al. 2009; Melis et al. 2010; Vennes et al. 2011; Debes et al. 2011; Xu & Jura 2012; Girven et al. 2012), offering clues to the fate of planetary systems when their host stars undergo post-main-sequence evolution. The most likely origin for the disks is the tidal disruption of asteroids (Graham et al. 1990; Debes & Sigurdsson 2002; Jura 2003), and the subsequent accretion of this tidally disrupted material can explain the large metal abundances in the white dwarf atmospheres.

The discovery of a gaseous disk around the hot white dwarf SDSS J1228+1040 (Gänsicke et al. 2006) and our subsequent identification of a dusty extension to that disk (Brinkworth et al. 2009) showed that debris disks are not restricted to low-temperature white dwarfs, as previously believed (Kilic et al. 2006), and dust and gas readily coexist in such a disk. Indeed, measured parameters for the 18 dusty white dwarfs (see Farihi et al. 2010 for an overview) show that the presence of dust does not appear to correlate with temperature.

Here, we present infrared photometry and spectral energy distribution (SED) modeling for a further four white dwarfs similar to SDSS J1228+1040: SDSS J104341.53+085558.2, SDSS J084539.17+225728.0, SDSS J161717.04+162022.4, and SDSS J073842.57+183509.6 (hereafter SDSS1043, SDSS0845, SDSS1617, and SDSS0738, respectively). As with SDSS J1228+1040, all have previously been identified from Sloan Digital Sky Survey (SDSS) spectroscopy, revealing Ca II 860 nm emission lines from a gaseous disk component (Gänsicke et al. 2007, 2008, 2011; B. T. Gänsicke et al. 2012, in preparation), leading us to search for an infrared excess indicative of dusty extensions to these disks. SDSS0738 was independently discovered by Dufour et al. (2010) because of extremely strong metal pollution. Dufour et al. (2010) also reported an infrared excess in the near-IR, but did not notice the Ca II emission of the gaseous disk component.

SDSS1228, SDSS1043, and SDSS1617 are all hydrogen-dominated DA white dwarfs, while SDSS0845 and SDSS0738 are helium-dominated DB white dwarfs. All are metal polluted, all are moderately "warm," with temperatures ranging from 13,000–22,000 K, and hence they are relatively young (cooling ages of ∼100–600 Myr).

2. OBSERVATIONS AND DATA REDUCTION

2.1. Spitzer Space Telescope

We were awarded 2.7 hr in Cycle 4 (P40048), 0.7 hr in Cycle 5 (P50118), and 2.5 hr in Cycle 7 (P70012) to search for a dusty component to the disks around our four targets (see Table 1 for a full list of observations). For SDSS1043, we obtained Infrared Array Camera (IRAC; see Fazio et al. 2005) data in all four channels (3.6–8.0 μm). For SDSS0845, we obtained IRAC data at 4.5 μm and 8.0 μm, Infrared Spectrograph (IRS; Houck et al. 2004) Blue Peak-Up Imaging at 16 μm, and Multiband Imaging Photometer (MIPS; Rieke et al. 2004) imaging at 24 μm. For SDSS1617 and SDSS0738, we obtained warm IRAC data at 3.6 μm and 4.5 μm.

The IRAC data reduction for all sources was carried out on the individual corrected basic calibrated data (CBCD; cbcd.fits) frames downloaded from the *Spitzer* archive. The CBCDs were initially combined with the standard SSC software, MOsaic and Point Source Extraction (MOPEX; Makovoz et al. 2006) with dual outlier rejection to create a single mosaicked image for

Table 1
Observation Log for *Spitzer Space Telescope* Data

Target	Instrument/ Channel	AOR Key	Total Integration Time (s)	Date	Pipeline
SDSS J0845+2257	IRAC Ch. 2	25459968	600	2008 May 9	S18.7
SDSS J0845+2257	IRAC Ch. 4	25459968	600	2008 May 9	S18.7
SDSS J0845+2257	IRS Blue PUI	25460224	600	2008 Dec 2	S18.7
SDSS J0845+2257	MIPS-24	25460480	140	2008 May 18	S18.12
SDSS J0845+2257	MIPS-24	25460736	140	2008 May 19	S18.12
SDSS J1043+0855	IRAC Ch. 1	22248448	3000	2008 Jun 10	S18.7
SDSS J1043+0855	IRAC Ch. 2	22248448	3000	2008 Jun 10	S18.7
SDSS J1043+0855	IRAC Ch. 3	22248448	3000	2008 Jun 10	S18.7
SDSS J1043+0855	IRAC Ch. 4	22248448	3000	2008 Jun 10	S18.7
SDSS J1617+1620	IRAC Ch. 1	39873024	750	2010 Sep 1	S18.18
SDSS J1617+1620	IRAC Ch. 2	39873024	750	2010 Sep 1	S18.18
SDSS J0738+1835	IRAC Ch. 1	39872768	3000	2010 Dec 1	S18.18
SDSS J0738+1835	IRAC Ch. 2	39872768	3000	2010 Dec 1	S18.18

each channel. This was used to determine the position of the target. All of the original downloaded CBCD frames were then corrected for array location dependence, using the correction frames supplied by the Spitzer Science Center (SSC). Aperture photometry was carried out on the corrected CBCD frames with IRAF, using an aperture radius of 3.0 pixels. The sky subtraction was applied using an annulus from 12 to 20 pixels in radius.

SDSS1043 was found to have a blended neighbor in the extraction aperture. We calculated the individual flux densities for each of the blended sources by measuring the combined flux, then splitting this by the ratio of peak brightness of a Gaussian fit to each source in each channel.

The IRAC photometry for all sources was then converted from MJy sr^{-1} to μJy, and aperture corrected using the standard aperture corrections provided by the SSC. We did not apply a pixel phase correction to the channel 1 data, but included an extra 1% in our error budget to account for this (Reach et al. 2005). No color correction was applied, since we quote the isophotal wavelengths, thus eliminating most of the color dependency of the flux calibration and rendering the magnitude of the correction negligible compared to our uncertainties. Uncertainties were estimated using the rms scatter in the photometry in the individual frames, divided by the square root of the number of frames. The quoted uncertainties are either our calculated uncertainty or the IRAC calibration uncertainty derived by Reach et al. (2005), whichever was larger.

The IRS Peak-Up Imaging and MIPS data for SDSS0845 were combined in much the same way, using MOPEX to create a mosaic to measure the source positions, and carrying out the photometry on the individual basic calibrated data frames. The sky background was found to be variable across the IRS Peak-Up array, and so we created a sky flat by combining all of the dithers and rejecting the sources. This sky flat was subtracted from the individual frames before carrying out the photometry, bringing the sky background to zero. The photometry for both the IRS and MIPS data was obtained via IRAF, using an aperture radius of 3.0 pixels with no sky subtraction for IRS, and an aperture radius of 3″ (1.224 pixels) with a background aperture of 20″–32″ for MIPS. After converting from MJy sr^{-1} to μJy, the flux densities were aperture corrected to the calibration apertures using the standard corrections provided by the SSC.

Finally, for all of the data for the four targets, we rejected the photometry from the original frames that had been flagged by the MOPEX dual outlier rejection algorithm. We take the unweighted mean of the remaining photometry in each channel as the quoted flux densities. An estimate of the uncertainties was measured using (rms scatter)/sqrt(number of frames), consistently giving uncertainties lower than the instrument calibration uncertainties. We therefore adopt the instrument calibration uncertainties from the SSC as the uncertainties on our data. For MIPS this is 4%, and for IRSPUI this is 5%.

2.2. AAT, SOFI, UKIDSS, GALEX, SDSS, 2MASS, and WISE Data

Near-infrared imaging of SDSS0845 was obtained at the Australian Astronomical Observatory's Anglo-Australian Telescope (AAT) using the InfraRed Imaging Spectrograph 2 on 2008 February 22, and retrieved from the public AAT archive. A nine-point dither pattern was used, with individual exposure times of 30 s, 42 s, and 67 s, and total exposure times of 270 s, 378 s, and 603 s in J, H, and K_s, respectively. SDSS1617 was observed in the K_s band on 2010 May 1 using SOFI on the ESO New Technology Telescope (NTT). A total of twenty 5 s images were obtained, offset randomly within a 15″ box. The data were sky-median subtracted, astrometrically calibrated using the WCSTools[5], and co-added using SWarp.[6] Object detection and the aperture photometry were done using the SExtractor (Bertin & Arnouts 1996). Instrumental magnitudes were converted to the Two Micron All Sky Survey (2MASS) system using a set of five bright stars near SDSS0845 and ten stars near SDSS1617. The uncertainty in the calibration is 0.02 mag in all bands, and was added in quadrature to the statistical uncertainties in the photometry. The J, H, and K_s magnitudes, fluxes, and uncertainties are reported in Table 2.

Observations of SDSS1043 in Y, J, H, and, K bands have been obtained with UKIRT/WFCAM as part of UKIDSS (Lawrence et al. 2007) on 2009 May 22 and December 15 (Table 2). The *Galaxy Evolution Explorer* (*GALEX*; Martin et al. 2005), SDSS (Abazajian et al. 2009), and 2MASS (Skrutskie et al. 2006) archives and the *Wide-field Infrared Survey Explorer* (*WISE*) Preliminary Data Release were searched for additional photometry of our targets. The archival and *WISE* photometry are also listed in Table 2.

2.3. Possible Contamination of SDSS J0845+2257

The NIRI imaging of SDSS0845 obtained by Melis et al. (2010) revealed the presence of a faint galaxy at a 1.″8 separation

[5] http://tdc-www.harvard.edu/wcstools
[6] http://www.astromatic.net

Table 2
Photometry for All Four Target Stars

Waveband	Wavelength	Flux Density (mJy)			
	(μm)	SDSS0738+1835	SDSS0845+2257	SDSS1043+0855	SDSS1617+1620
GALEX FUV	0.158	$0.061^{+11\%}_{-12\%}$	$1.92 \pm 5\%$	$0.66 \pm 5\%$	$0.345^{+4.2\%}_{-4.4\%}$
GALEX NUV	0.227	$0.161^{+4.7\%}_{-4.9\%}$	$2.28 \pm 5\%$	$0.54 \pm 5\%$	$0.406^{+1.7\%}_{-1.8\%}$
Y	1.02	...	...	$0.182^{+4.9\%}_{-4.4\%}$ (b)	...
J	1.2	...	$0.473 \pm 11\%$ (a)	$0.128^{+6.3\%}_{-5.4\%}$ (b)	...
H	1.6	...	$0.349 \pm 14\%$ (a)	$0.088^{+7.4\%}_{-6.9\%}$ (b)	...
K	2.2	...	$0.294 \pm 17\%$ (a)	$0.049^{+13\%}_{-12\%}$ (b)	$0.122^{+8.8\%}_{-9.6\%}$ (c)
WISE-1	3.35	...	$0.267 \pm 4.5\%$	...	$0.104 \pm 7.7\%$
IRAC-1	3.550	$0.082 \pm 3\%$	...	$0.039 \pm 6\%$	$0.108 \pm 3\%$
IRAC-2	4.493	$0.075 \pm 3.7\%$	$0.248^{+3\%}_{-4\%}$	$0.025 \pm 8\%$	$0.095 \pm 3\%$
WISE-2	4.60	...	$0.237 \pm 8.9\%$	...	$0.097 \pm 15.5\%$
IRAC-3	5.731	...	...	$0.017 \pm 16\%$	...
IRAC-4	7.872	...	$0.179^{+21\%}_{-24\%}$	$0.029 \pm 27\%$	...
IRS PU-16	15.60	...	$0.151^{+3.6\%}_{-4.7\%}$	...	...
MIPS-24	23.68	...	$0.111^{+4\%}_{-4\%}$	...	...

Note. Source of NIR photometry: (a) AAT, (b) UKIDSS, and (c) SOFI.

northeast of the white dwarf. We have downloaded the NIRI *J*-, *H*-, and K_s-band images of SDSS0845 from the Gemini Science Archive and, after correction for nonlinearity using the python scripts provided by Gemini, processed them in the same manner as the AAT and NTT data described above. In order to measure the relative contributions of the star and the galaxy, first an annulus was defined, centered on the star, with inner and outer radii of 4″ and 7″ on the sky (large enough to avoid the galaxy) to measure the sky background. The star's contribution was then measured from the flux summed over a 1.″6 diameter aperture, while the galaxy's flux was measured from the union of pixels covered by three overlapping circular apertures covering its major axis. To estimate the degree to which the galaxy flux was contaminated by light from the star, three identical control apertures were placed diametrically opposite to the galaxy apertures relative to the star. The instrumental magnitudes were photometrically calibrated using a bright 2MASS star in the field. We find $J = 16.44 \pm 0.05$, $H = 16.30 \pm 0.06$, and $K = 16.04 \pm 0.07$ for SDSS0845, and $J = 20.33 \pm 0.79$, $H = 19.29 \pm 0.32$, and $K = 18.65 \pm 0.24$ for the nearby galaxy. These results agree well with the NIRI magnitudes of Melis et al. (2010), apart from the fact that we have somewhat larger uncertainties.

To estimate the contamination of the galaxy in the *Spitzer* beam, we obtained the galaxy SEDs of Maraston (1998, 2005) based on the initial mass function of Kroupa (2001). We then redshifted all galaxy SEDs by redshifts $0 \leqslant z \leqslant 3$, in steps of 0.2, and discarded all combinations of redshift and age that would disagree with the observed $J - H$ and $H - K_s$ colors and the apparent K_s magnitude. The NIRI data constrain the redshift of the galaxy to $1.4 \lesssim z \lesssim 3.0$, with the range 2.4–3.0 only feasible for young (<1 Gyr) galaxies. The spatial extension of the galaxy is suggestive of a redshift at the lower end of the range allowed by the NIRI photometry (Ferguson et al. 2004).

The contribution of the galaxy to the IRAC-1 and -2 channels is 0.04 ± 0.01 mJy and 0.05 ± 0.01 mJy, relatively independent of the galaxy type. The maximum contribution in the IRAC-3 and -4 channels is ∼8 mJy for a young (<1 Gyr) high-redshift ($z \sim 3$) galaxy. However, given the combined constraint from morphology and near-infrared photometry, the contribution of the galaxy to the IRAC-3 and -4 channels is likely to be <5 mJy. Galaxy models are poorly constrained in the mid-IR, and so we are unable to learn anything more about the galaxy from the IRS-PU and MIPS channels, other than the fact that the galaxy flux continues to drop out to longer wavelengths. At these longer wavelengths, the SED is dominated by the flux density from the dust disk. In Figure 2, we show an 8 Gyr old, redshift $z = 1.6$ galaxy as an example of the flux contribution to the *Spitzer* bands.

3. RESULTS AND MODELING

We plotted the SEDs of the four white dwarfs, comparing them to models of isolated white dwarfs and other system components as described below. We define an infrared excess as significant if any of the infrared photometric points lies more than 3σ above the model of the white dwarf.

Where we detect an infrared excess, we attempt to model it using an optically thick, geometrically thin dusty disk, with a temperature profile $T_{\rm disk} \propto r^{-\beta}$ where $\beta = 3/4$ (Jura 2003), as previously described in Brinkworth et al. (2009). The ratio of stellar radius to distance sets the absolute scale of the white dwarf photospheric flux and is fixed in our modeling based on the best available parameters. The free parameters in the model are the inner disk radius ($R_{\rm in}$), the outer disk radius ($R_{\rm out}$), and the disk inclination (i). A grid of disk models was calculated with inner ($T_{\rm in}$) and outer ($T_{\rm out}$) disk temperatures, each corresponding to a value of $R_{\rm in}$ and $R_{\rm out}$ ranging from 100 to 1800 K in steps of 50 K, and inclination ranging from 0° to 90° in steps of 5°. $T_{\rm out}$ was fixed to be cooler than $T_{\rm in}$. A least χ^2 method was used to fit the *H*-, *K*-, and IRAC-band infrared fluxes. See Girven et al. (2012) for further information on the fitting technique.

The model is plotted as a dash-dotted gray line in the figures. For each of our white dwarf targets, we include two figures: one showing the best-fit model to the data points, regardless of physical feasibility, and one showing the closest possible physical model to that best fit. Analyses of the photospheric abundances of white dwarfs hosting dusty disks suggest that the bulk composition of the circumstellar material is dominated

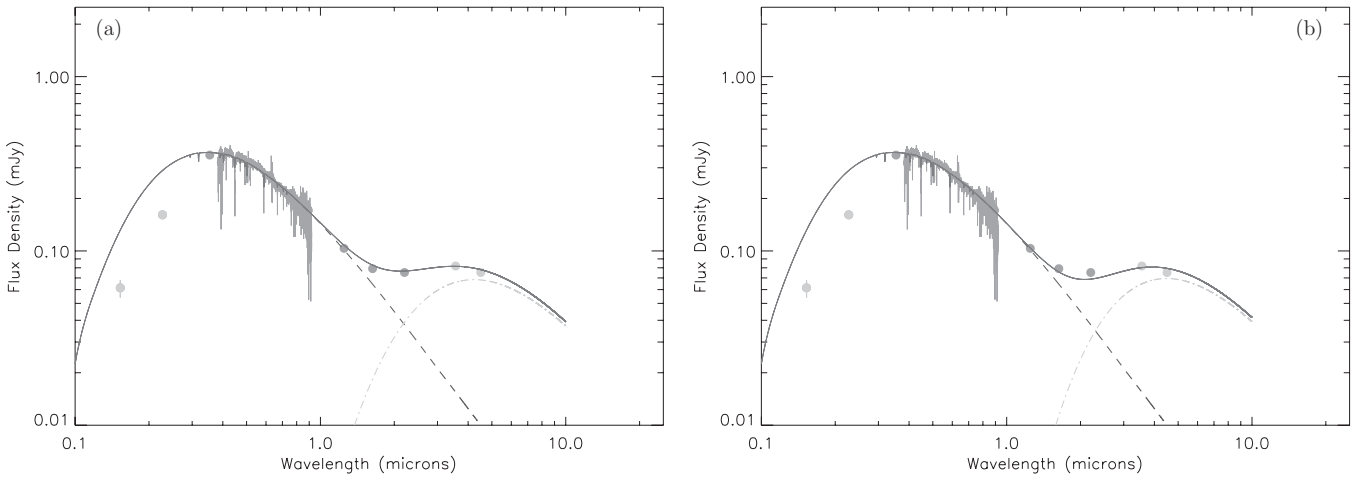

Figure 1. Spectral energy distribution (SED) of SDSS J0738+1835 from the ultraviolet to the mid-infrared. See Table 2 for the *GALEX* and *Spitzer* data. The white dwarf spectrum was taken from the SDSS Data Release 7 and is plotted along with the *GALEX*, *Spitzer*, *WISE*, and SDSS photometry, and the near-IR data from Dufour et al. (2010). The SED shows a significant flux density excess above that expected from the white dwarf alone. The SED on the left is compared to a white dwarf + optically thick disk model with an inner dust temperature of 1800 K, an outer disk temperature of 830 K, and an inclination of 58°. The SED on the right limits the inner disk temperature to $T_{\rm in} = 1400$ K, with $T_{\rm out} = 930$ K and a face-on inclination of 0°. See Section 3.1 for the full range of possible models.

Table 3
Stellar Parameters for Target Stars

Parameter	SDSS J0738+1835	SDSS J0845+2257	SDSS J1043+0855	SDSS J1617+1620
White dwarf temperature (K)	13600	18600	17912	13432
Distance (pc)	120	85	183	122
log(g)	8.5	8.2	8.0	8.0
Radius (cm)	6.16e8	6.27e8	9.05e8	8.77e8

by Mg, O, Si, and Fe, similar to the bulk composition of the Earth (Zuckerman et al. 2007; Klein et al. 2011). The condensation temperature of the main minerals carrying these elements is 1400 K (Lodders 2003), and we therefore do not expect that dusty debris disks around white dwarfs can survive temperatures much above that. Hence, we define an inner dust disk temperature of 1400 K as a physical limit. For each target, we also describe the coolest inner disk temperature that we were able to match to the data while staying consistent to within 3σ of all the data points.

3.1. SDSS J0738+1835

The flux densities from *GALEX* and *Spitzer* are given in Table 2, and are plotted in light gray in Figure 1, along with the SDSS DR7 spectrum (gray line). We also included near-IR photometry from Dufour et al. (2010), also plotted in dark gray. The DB white dwarf model is shown as a dashed black line, with $T_{\rm eff} = 13{,}600$ K, log(g) = 8.5, $R_{\rm WD} = 0.00886\ R_{\odot}$ (Table 3; see Dufour et al. 2010). We use a distance of $d = 120$ pc, rather than the 136 ± 22 pc quoted in Dufour et al. (2010), as this gives a better fit to the white dwarf SED. This is still consistent with the Dufour et al. value.

The photometry of SDSS0738 shows a clear flux density excess in the infrared wavelengths, compared to the white dwarf model. The best-fitting disk model (Figure 1(a)) has $T_{\rm in} = 1800$ K, $T_{\rm out} = 830$ K, and an inclination of 60°, which is consistent with the modeling results from Dufour et al. (2010). The best physically motivated model with $T_{\rm in} = 1400$ K has $T_{\rm out} = 930$ K and a face-on inclination of 0° (Figure 1(b)). This corresponds to inner and outer disk radii of $R_{\rm in} = 12.4\ R_{\rm WD}$ ($0.11\ R_{\odot}$) and $R_{\rm out} = 21.3\ R_{\rm WD}$ ($0.19\ R_{\odot}$). The coolest possible inner disk temperature is constrained by the need for a high enough flux density to match the *JHK* data points, and has $T_{\rm in} = 1350$ K, $T_{\rm out} = 880$ K, and an inclination of 0°. These models are both consistent with the modeling carried out by Dufour et al. (2012), who used $T_{\rm in} = 1600 \pm 100$ K, $T_{\rm out} = 900 + 100/-200$ K, and an inclination of $40° \pm 20°$.

Analysis of the Ca II emission lines gives an outer radius of the gaseous disk component of $R_{\rm out} \simeq 1\ R_{\odot} \sin^2 i$, i.e., a maximum value of $R_{\rm out} \sim 110 R_{\rm WD}$ (B. T. Gänsicke et al. 2012, in preparation). While the Ca II emission lines provide no formal lower limit on $R_{\rm out}$, a low-inclination, practically face-on geometry seems unlikely, as it would imply a very narrow ring for the gaseous component, narrower than the dusty component.

3.2. SDSS J0845+2257

The *GALEX*, AAT, and *Spitzer* photometry for SDSS0845 are given in Table 2, and are plotted in light gray in Figure 2, along with the SDSS DR7 spectrum, SDSS photometry, NIR photometry from Melis et al. (2010) and Farihi et al. (2010), and the *WISE* Preliminary Data Release (dark gray). The data show a clear excess at wavelengths longer than $2\,\mu$m, above the flux density expected from the white dwarf and the contaminating background galaxy. For the white dwarf contribution, we adopted a DB model with $T_{\rm eff} = 18{,}621$ K, log(g) = 8.2, $d = 85$ pc, and $R_{\rm WD} = 0.009\ R_{\odot}$. The resultant model is plotted as a dashed gray line, while the white dwarf model with the background galaxy added is shown as a dash-dot-dot-dot line.

The models for SDSS0845 are shown in Figure 2. The first shows the best-fitting disk model, with an inner temperature of 1800 K, an outer temperature of 250 K, and an inclination of 85°. Figure 2(b) shows the closest physical model with an inner disk temperature constrained to 1400 K, $T_{\rm out} = 400$ K,

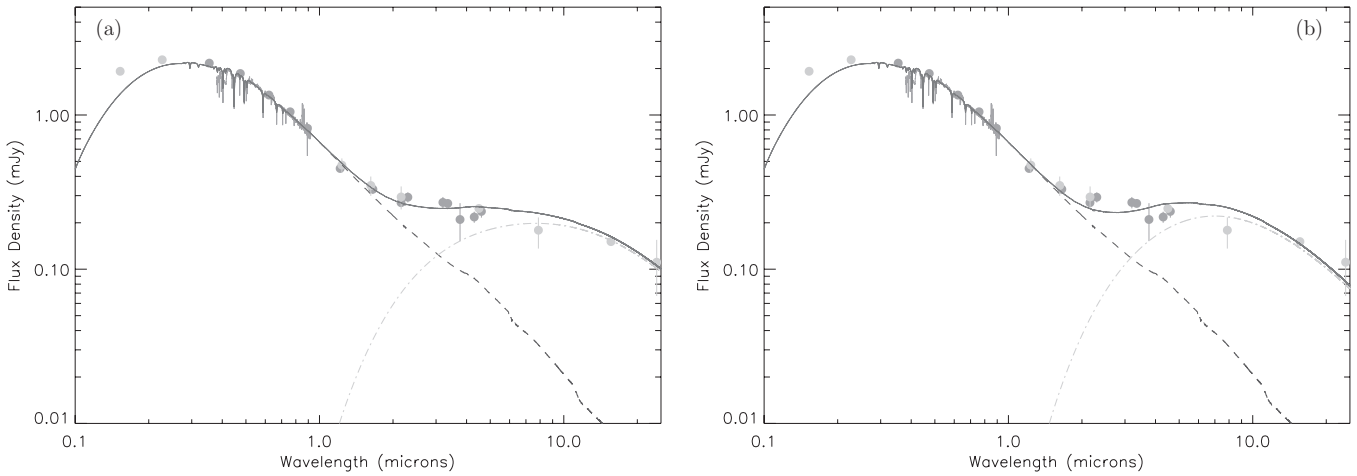

Figure 2. SED for SDSS J0845+2257 from the ultraviolet to the mid-infrared. *GALEX*, AAT, and *Spitzer* data are plotted in light gray, while SDSS, NIR (Melis et al. 2010), *AKARI* (Farihi et al. 2010), and *WISE* Preliminary Data Release photometry are plotted in dark gray, along with the SDSS DR7 white dwarf spectrum. The white dwarf model plus background galaxy (8 Gyr, $z = 1.6$; Maraston et al. (1998); Maraston (2005); see Section 2.3) is plotted in dash-dot-dot-dot. The SED shows a significant flux density excess from the K band to longer wavelengths, over the flux density expected from the white dwarf and the background galaxy alone. The SED on the left is compared with the best model of a white dwarf + background galaxy + optically thick dust disk with an inner dust temperature of 1800 K and an outer disk temperature of 250 K. The disk inclination is 83°. We note that, while this is a good fit, the inner dust temperature is above the expected dust sublimation temperature. The SED on the right is compared to the same model but with a physically possible inner dust disk temperature of 1400 K, an outer disk temperature of 400 K, and an inclination of 80°. See Section 3.2 for the full range of possible model parameters.

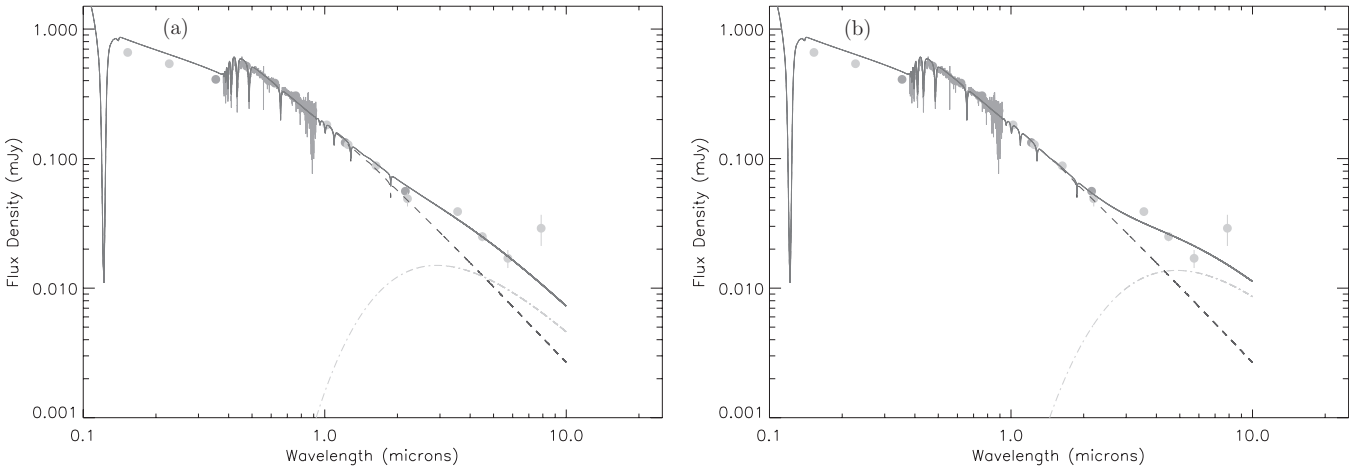

Figure 3. SED of SDSS 1043+0855 from the ultraviolet to the mid-infrared. The white dwarf spectrum was taken from SDSS Data Release 7 and is plotted along with the *GALEX*, UKIDSS, and *Spitzer* in light gray, and the SDSS photometry and NIR data from Melis et al. (2010) in dark gray. The SED shows a significant flux density excess above that expected from the white dwarf alone. The SED on the left is compared to a white dwarf + optically thick disk model with an inner dust temperature of 1800 K, an outer disk temperature of 1700 K, and an inclination of 40°. The SED on the right limits the inner disk temperature to $T_{\rm in} = 1400$ K, with $T_{\rm out} = 800$ K and an inclination of 85°. See Section 3.3 for the full range of possible models.

and inclination = 80°. This corresponds with inner and outer disk radii of $R_{\rm in} = 18.8\ R_{\rm WD}$ (0.17 $R_\odot$) and $R_{\rm out} = 99.7\ R_{\rm WD}$ (0.89 $R_\odot$). The coolest disk model still within 3σ of the plotted data points has $T_{\rm in} = 1100$ K, $T_{\rm out} = 600$ K, and an inclination of 70°.

The outer radius of the gaseous component was estimated by Gänsicke et al. (2008) to be ~0.8–0.9 $R_\odot$, which is comparable to that of the dust disk derived above.

3.3. SDSS J1043+0855

The *GALEX*, UKIDSS, and *Spitzer* flux densities for SDSS1043 are given in Table 2, and are plotted in Figure 3 together with the SDSS DR7 spectrum. The uncertainties on the *Spitzer* photometry for SDSS1043 are notably large, due to the faint nature of the source (only 30 μJy in IRAC channel 1). In addition to these data points, we include Canada–France–Hawaii Telescope and Lick near-IR photometry from Melis et al. (2010) to constrain our model. All previously published data are shown in dark gray in Figure 3, while the *GALEX*, UKIDSS, and *Spitzer* data are shown in light gray. We have fitted the DR7 spectrum of SDSS1043 using DA model spectra computed with the code of Koester (2010), which incorporates the updated Stark broadening calculations of Tremblay & Bergeron (2009), and find $T_{\rm eff} = 17912 \pm 362$ K and $\log(g) = 8.07 \pm 0.08$, corresponding to $M_{\rm WD} = 0.66 \pm 0.05\ M_\odot$ and $R_{\rm WD} = (8.67 \pm 0.47) \times 10^8$ cm (Table 3). These values are, within the uncertainties, consistent with those derived from the DR4 spectrum by Gänsicke et al. (2007), but given the improvement in the SDSS data reduction and line broadening, the new values reported here should be preferred.

The IRAC data points show a 3σ excess above the expected flux density of the white dwarf, increasing dramatically at 8 μm.

As with the other targets, we show the best-fit optically thick dust disk model in Figure 3(a), with an inner disk dust temperature of $T_{\rm in} = 1800$ K, $T_{\rm out} = 1700$ K, and an inclination of 40°. When constraining the inner disk temperature below the

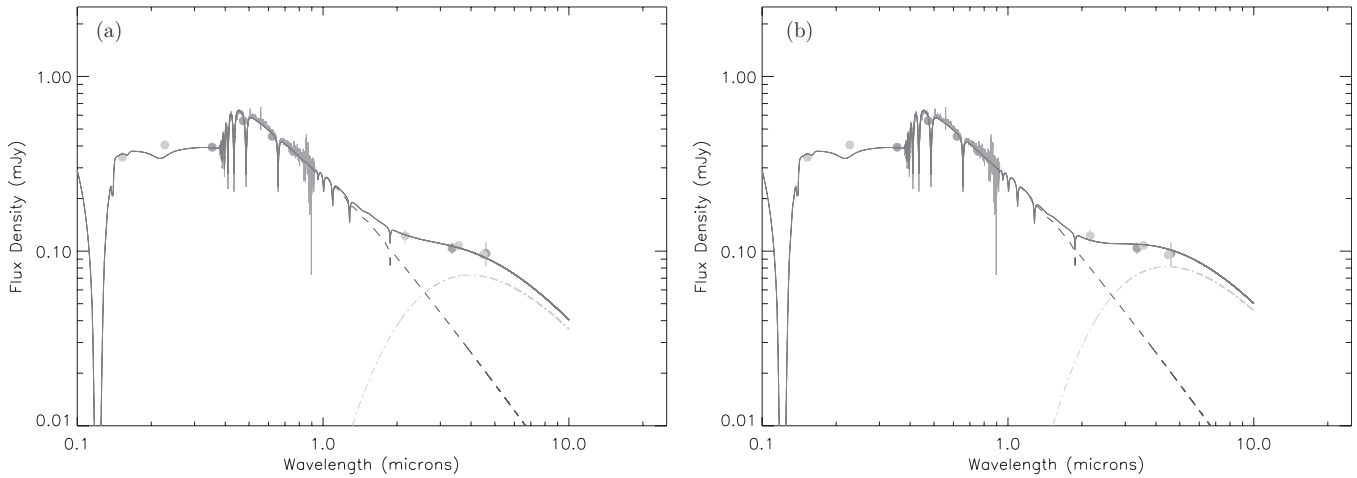

Figure 4. SED for SDSS J1617+1620 from the ultraviolet to the mid-infrared. *Spitzer*, *GALEX*, *WISE*, and SOFI data are reported in Table 2. *GALEX*, SOFI, and *Spitzer* data are plotted in light gray, while the SDSS data and the *WISE* Preliminary Data Release are shown in dark gray. The white dwarf spectrum was taken from SDSS Data Release 7. The SED shows a significant flux density excess from the *K* band to longer wavelengths, over the flux density expected from the white dwarf alone. The SED on the left is compared to the best-fit white dwarf + optically thick disk model with an inner dust temperature of 1800 K, an outer disk temperature of 950 K, and an inclination of 70°. The SED on the right limits $T_{\rm in}$ to 1400 K with $T_{\rm out} = 950$ K and $i = 50°$. See Section 3.4 for the full range of model parameters.

sublimation threshold of 1400 K, we find a best-fit model with $T_{\rm in} = 1400$, $T_{\rm out} = 800$ K, and $i = 85°$. This corresponds with inner and outer disk radii of $R_{\rm in} = 17.9\ R_{\rm WD}$ ($0.23\ R_\odot$) and $R_{\rm out} = 37.6\ R_{\rm WD}$ ($0.49\ R_\odot$). The coolest model allowed by the fit has $T_{\rm in} = 900$ K, $T_{\rm out} = 800$ K, and $i = 56°$.

Modeling the double-peaked Ca II line profiles, B. T. Gänsicke et al. (2012, in preparation) find, similar as for SDSS0738 and SDSS0845, $R_{\rm max} \sim 1\ R_\odot$ (see also Melis et al. 2010).

3.4. SDSS J1617+1620

The flux densities from *GALEX*, SOFI, and *Spitzer* are given in Table 2, and are plotted in light gray in Figure 4, together with the SDSS DR7 spectrum (dark gray). The data show a clear excess above the flux density from the white dwarf at the *Spitzer* wavelengths. The white dwarf model, also based on Gänsicke et al. (2011), is shown as a dashed black line and is a DA white dwarf model, with $T_{\rm eff} = 13{,}432$ K, $\log(g) = 8.04$, $d = 122$ pc, $R_{\rm WD} = 0.01261\ R_\odot$, reddened by $E(B-V) = 0.04$ to better match the optical SDSS spectrum. The reddening has a negligible effect at infrared wavelengths.

The best-fit dust disk model has an inner disk effective temperature $T_{\rm in} = 1800$ K, outer disk $T_{\rm out} = 950$ K, and an inclination of 70°, plotted as a gray dash-dotted line in Figure 4(a). The closest fit with $T_{\rm in}$ fixed at 1400 K has $T_{\rm out} = 950$ K and $i = 50°$ (Figure 4(b)). This corresponds with inner and outer disk radii of $R_{\rm in} = 12.2\ R_{\rm WD}$ ($0.15\ R_\odot$) and $R_{\rm out} = 20.4\ R_{\rm WD}$ ($0.26\ R_\odot$). The model with the coolest possible inner disk temperature has $T_{\rm in} = 1100$ K, $T_{\rm out} = 620$ K, and $i = 53°$.

The peak separation of the Ca II emission lines implies a maximum outer radius of the gaseous component of $90\ R_{\rm WD}$ (B. T. Gänsicke et al. 2012, in preparation).

4. DISCUSSION AND CONCLUSIONS

We find that out of these four white dwarfs with previously identified gaseous disks, all show evidence for dusty extensions to those disks, as seen in the previously studied SDSS J1228+1040. We note that the best-fitting models for all of these disks have inner disk temperatures hotter than the sublimation temperature expected from the bulk composition of the dust, although all can be modeled satisfactorily with inner disk temperatures fixed to a physically more plausible temperature of 1400 K. When adding in the results from our previous study of SDSS1228 (Brinkworth et al. 2009), we find that all five white dwarfs with Ca II emission from a gaseous debris disk also show dusty components to those disks. It is evident that gaseous and dusty debris disks easily coexist around white dwarfs, and the dusty disks likely feed the gaseous component. Both Jura (2008) and Melis et al. (2010) suggest that dust disks are a pre-requisite to gaseous disks, and our findings are consistent with that evolutionary path, and vice versa, the presence of gas is likely to have a major effect on the evolution of the planetary debris disks around white dwarfs (Rafikov 2011b).

The one outlier of our sample is SDSS1043. Even taking the uncertainties on the photometry into account, it is apparent that the dust in the system is far less pronounced than in the other three targets, despite very similar gaseous disk signatures in all four systems. The 4.5 μm excesses seen in SDSS0738, SDSS0845, and SDSS1617 are 7.5, 5.7, and 4.5 times the white dwarf contribution, respectively. In contrast, in SDSS1043, the measured flux density at 4.5 μm is only 1.7 times the white dwarf contribution. Why SDSS1043 should lack significant dust compared to the other three systems remains a mystery. Maybe the system is at a higher inclination, so we are seeing the correspondingly smaller projected area of the edge of the geometrically thin disk, rather than its face, but this does not seem to be borne out in the modeling of the other systems. Considering the likelihood that the dust disks feed the gaseous disks in these systems, it is feasible that we are seeing the tail end of an asteroidal tidal disruption event that took place at an earlier time than the other systems, such that the dust around SDSS1043 is now depleted compared to the other three white dwarfs, and the gaseous disk dominates the SED. This seems consistent with the most recent estimates for disk lifetimes: a massive ($\sim 10^{22}$) disk accreting due to Poynting–Robertson drag alone can be expected to survive for several Myr (Rafokov 2011a). However, when a gas disk is present in the system due to sublimation of the inner disk, runaway accretion can occur. Rafikov (2011b) predicts that this can lead to the disk being exhausted in $\sim 10^5$ yr. Bochkarev & Rafikov (2011) extend this analysis to include gas generated from multiple asteroid impacts, in which they confirm

the estimated disk lifetime of several Myr. On the other hand, Debes (2011) calculates that dust disks around white dwarfs may last for up to 1 Gyr, while gas disks that are not being replenished are unlikely to last more than 10^4 years before fully accreting onto the white dwarf. If the disk around SDSS1043 is indeed reaching the end of its lifetime, then long-term infrared monitoring of the SEDs of all of the five systems (SDSS1228, SDSS0738, SDSS0845, SDSS1043, and SDSS1617) over the next few decades may help to shed some light on this.

The authors thank the referee for detailed and useful comments that helped to improve this paper.

The DA white dwarf models used in the analysis were calculated with the modified Stark broadening profiles of Tremblay & Bergeron (2009), kindly made available by the authors.

Co-authors Gaensicke and Marsh were supported by an STFC rolling grant.

This work is based on observations made with the *Spitzer Space Telescope*, which is operated by the Jet Propulsion Laboratory, Caltech, under NASA contracts 1407 and 960785. This work makes use of data products from the Two Micron All Sky Survey, which is a joint project of the University of Massachusetts and IPAC/Caltech, funded by NASA and the NSF. The SOFI results in this paper are based on observations collected at the European Southern Observatory (La Silla) under program ID 085.D-0541. This publication makes use of data products from the *Wide-field Infrared Survey Explorer*, which is a joint project of the University of California, Los Angeles, and the Jet Propulsion Laboratory/California Institute of Technology, funded by the National Aeronautics and Space Administration. Funding for the SDSS and SDSS-II has been provided by the Alfred P. Sloan Foundation, the Participating Institutions, the National Science Foundation, the U. S. Department of Energy, the National Aeronautics and Space Administration, the Japanese Monbukagakusho, the Max Planck Society, and the Higher Education Funding Council for England. The SDSS Web site is http://www.sdss.org/. The SDSS is managed by a very long list of institutions, who can all be found at the following Web site: http://www.sdss.org/collaboration/credits.html.

This research has made use of NASA's Astrophysics Data System. This research has made use of the SIMBAD database, operated at CDS, Strasbourg, France.

REFERENCES

Abazajian, K. N., Adelman-McCarthy, J. K., Agüeros, M. A., et al. 2009, ApJS, 182, 543
Becklin, E. E., Farihi, J., Jura, M., et al. 2005, ApJ, 632, L119
Bertin, E., & Arnouts, S. 1996, A&AS, 117, 393
Bochkarev, K. V., & Rafikov, R. 2011, ApJ, 741, 36
Brinkworth, C. S., Gänsicke, B. T., Marsh, T. R., Hoard, D. W., & Tappert, C. 2009, ApJ, 696, 1402
Debes, J. 2011, in White Dwarf Atmospheres and Circumstellar Environments, ed. D. W. Hoard (Weinhein, Germany: Wiley-VCH)
Debes, J. H., Hoard, D. W., Kilic, M., et al. 2011, ApJ, 729, 4
Debes, J. H., & Sigurdsson, S. 2002, ApJ, 572, 556
Dufour, P., Kilic, M., Fontaine, G., et al. 2010, ApJ, 719, 803
Dufour, P., Kilic, M., Fontaine, G., et al. 2012, ApJ, accepted (arXiv:1201.6252)
Farihi, J., Gänsicke, B. T., Steele, P. R., et al. 2012, MNRAS, in press
Farihi, J., Jura, M., Lee, J.-E., & Zuckerman, B. 2010, ApJ, 714, 1386
Farihi, J., Jura, M., & Zuckerman, B. 2009, ApJ, 694, 805
Farihi, J., Zuckerman, B., & Becklin, E. E. 2008, ApJ, 674, 431
Fazio, G. G., Hora, J. L., Allen, L. E., et al. 2005, ApJS, 154, 10
Ferguson, H. C., Dickinson, M., Giavalisco, M., et al. 2004, ApJ, 600, L107
Gänsicke, B. T. 2011, in AIP Conf. Proc. 1331, Planetary Systems Beyond the Main Sequence, ed. S. Schuh, H. Drechsel, & U. Heber (Melville, NY: AIP), 211
Gänsicke, B. T., Koester, D., Marsh., T. R., Rebassa-Mansergas, A., & Southworth, J. 2008, MNRAS, 391, L103
Gänsicke, B. T., Marsh, T. R., & Southworth, J. 2007, MNRAS, 380, L35
Gänsicke, B. T., Marsh, T. R., Southworth, J., & Rebassa-Mansergas, A. 2006, Science, 314, 1908
Girven, J., Brinkworth, C. S., Farihi, J., et al. 2012, ApJ, accepted (arXiv:1202.3784v1)
Graham, J. R., Matthews, K., Neugebauer, G., & Soifer, B. T. 1990, ApJ, 357, 216
Houck, J. R., Charmandaris, V., Brandl, B. R., et al. 2004, ApJS, 154, 211
Jura, M. 2003, ApJ, 584, L91
Jura, M. 2008, AJ, 135, 1785
Jura, M., Farihi, J., & Zuckerman, B. 2007, ApJ, 663, 1285
Kilic, M., Patterson, A. J., Barber, S., Leggett, S. K., & Dufour, P. 2011, MNRAS, 419, L59
Kilic, M., & Redfield, S. 2007, ApJ, 660, 641
Kilic, M., von Hippel, T., Leggett, S. K., & Winget, D. E. 2005, ApJ, 632, L115
Kilic, M., von Hippel, T., Leggett, S. K., & Winget, D. E. 2006, ApJ, 646, 474
Klein, B., Jura, M., Koester, D., & Zuckerman, B. 2011, ApJ, 741, 64K
Koester, D. 2010, Mem. Soc. Astron. Ital., 81, 921
Kroupa, P. 2001, MNRAS, 322, 231
Lawrence, A., Warren, S. J., Almaini, O., et al. 2007, MNRAS, 379, 1599
Lodders., K. 2003, ApJ, 591, 1220
Makovoz, D., Roby, T., Khan, I., & Booth, H. 2006, Proc. SPIE, 6274, 10
Maraston, C. 1998, MNRAS, 300, 872
Maraston, C. 2005, MNRAS, 362, 799
Martin, D. C., Fanson, J., Schiminovich, D., et al. 2005, ApJ, 619, 1
Melis, C., Jura, M., Albert, L., Klein, B., & Zuckerman, B. 2010, ApJ, 722, 1078
Rafikov, R. 2011a, ApJ, 732, L3
Rafikov, R. 2011b, MNRAS, 416, L55
Reach, W. T., Kuchner, M. J., von Hippel, T., et al. 2005, ApJ, 635, L161
Rieke, G. H., Young, E. T., Engelbracht, C. W., et al. 2004, ApJS, 154, 25
Skrutskie, M. F., Cutri, R. M., Stiening, R., et al. 2006, AJ, 131, 1163
Telesco, C. M., Joy, M., & Sisk, C. 1990, ApJ, 358, L17
Tokunaga, A. T., Becklin, E. E., & Zuckerman, B. 1990, ApJ, 358, L21
Tremblay, P.-E., & Bergeron, P. 2009, ApJ, 696, 1755
Vennes, S., Kawka, A., & Németh, P. 2011, MNRAS, 413, 2545
von Hippel, T., Kuchner, M. J., Kilic, M., Mullally, F., & Reach, W. T. 2007, ApJ, 662, 544
Xu, S., & Jura, M. 2012, ApJ, 745, 88
Zuckerman, B., & Becklin, E. E. 1987, Nature, 330, 138
Zuckerman, B., Koester, D., Melis, C., Hansen, B. M., & Jura, M. 2007, ApJ, 671, 872